Catalysis Today 176 (2011) 453–457

Contents lists available at ScienceDirect

Catalysis Today

journal homepage: www.elsevier.com/locate/cattod

Ceria–zirconia mixed oxides as thermal resistant catalysts for the decomposition of nitrous oxide at high temperature

P. Esteves[a], Y. Wu[a], C. Dujardin[a], M.K. Dongare[b], P. Granger[a,*]

[a] Université Lille Nord de France, Université de Lille 1, Unité de Catalyse et de Chimie du Solide UMR 8181, Cité scientifique, Bâtiment C3, 59655 Villeneuve d'Ascq, France
[b] Catalysis and Inorganic Chemistry Division, National Chemical Laboratory, Pune 411008, India

ARTICLE INFO

Article history:
Received 27 August 2010
Received in revised form 13 October 2010
Accepted 17 October 2010
Available online 3 December 2010

Keywords:
Greenhouse gas
Nitrous oxide
N_2O catalytic decomposition
Ceria–zirconia based catalysts
Nitric acid plant

ABSTRACT

This present study deals with the development of thermally stable catalysts for the decomposition of nitrous oxide. There is actually a growing interest to minimise the emissions of nitrous oxide (N_2O) as side-product from nitric acid plants due to a global warming potential of approximately 300 times higher than that of CO_2. Different strategies have already been implemented at industrial scale but they are still suffering from significant drawbacks essentially associated to a poor selectivity and sometimes a short lifetime in particular when the catalytic process is inserted downstream the ammonia burner. In those critical conditions, with high residual temperature of ~900 °C, significant surface and bulk reconstructions take place and then lead to drastic losses of specific surface area and related catalytic performances in the decomposition of N_2O to N_2. Previous investigations performed in our laboratory revealed the potentiality of zirconia particularly after yttria incorporation [Appl. Catal. B 62 (2005) 236]. Novel developments of more stable ceria–zirconia based catalysts are reported in this study. Further stabilisation and enhancement in activity have been discussed on the basis of oxygen mobility related to structural properties.

1. Introduction

Unregulated nitrous oxide (N_2O) emissions might be considered as a serious drawback because of a much higher global warming potential than CO_2 and a longer lifetime. Consequently, the contribution of N_2O to the green house effect might be significant even at very low concentration contrary to CO_2. Among the different sources already identified [1–3], the abatement of N_2O emissions from industrial plants is probably the most feasible by implementing catalytic processes instead of thermal ones. First attempts led to successful developments for adipic acid plants [3,4]. Under industrial gas stream, bulk and support Cu-containing perovskite based materials were found very active towards the catalytic N_2O decomposition [4]. Now, particular attention is paid to N_2O as undesirable by-product from the catalytic oxidation of ammonia into nitric oxide particularly on aged platinum–rhodium gauzes. Pérez-Ramirez et al. [3,5,6] extensively investigated the different strategies for controlling N_2O emissions and classified different varieties of catalytic abatement processes. Among the different options, one can distinguish secondary abatement processes set up between the ammonia burner and the absorber which strongly differ from quaternary abatement involving end-of-pipe catalytic solutions with rather low running temperatures in comparison with the previous option. The simultaneous conversion of N_2O and NO is usually a challenging task for quaternary abatement processes particularly in the presence of an excess of oxygen and the use of a reducing agent is usually a prerequisite step [7–11]. High temperature catalytic processes represent an important issue of practical interest with the decomposition of N_2O in the absence of ammonia. However, such a technology still suffers from significant drawbacks associated with the poor stability of the catalysts [12–18]. Catalytic processes downstream from the ammonia burner are exposed to high residual temperature ($T \cong 900$ °C) and large amounts of water which favour thermal sintering reactions and induce deactivation phenomena then limiting the durability of such processes. Different patents have already been claimed for high temperature applications [15–17]. The selectivity is also an important issue because parallel to N_2O conversion, the catalyst must be inactive towards the conversion of NO_x to avoid subsequent loss of HNO_3 yield. Among different variety of catalysts, Fe and Mn substituted hexaaluminates [5,6] or ceramic Ca aluminate [19] was found to be promising for high temperature abatement of N_2O in chemical industry. Also, Fe_2O_3/Al_2O_3 exhibits a high activity in a pilot-plant reactor and very good thermal stability [20]. This study reports an investigation at the lab-scale of ceria-induced effect on the catalytic properties of zirconia. Such mixed oxides, currently used for three-way applications [21–25] are recognised to exhibit high resistance to thermal sintering and high oxygen mobility. Hence,

* Corresponding author. Tel.: +33 3 20 43 49 38; fax: +33 3 20 43 65 61.
E-mail address: pascal.granger@univ-lille1.fr (P. Granger).

0920-5861/$ – see front matter © 2010 Elsevier B.V. All rights reserved.
doi:10.1016/j.cattod.2010.10.068

further enhancement of the oxygen storage capacity could induce better performances in the decomposition of N_2O as suggested elsewhere [4]. Particular attention was paid to the mode of Ce incorporation in order to stabilise solid solutions and to relate textural and structural properties to catalytic properties.

2. Experimental

Ceria–zirconia mixed oxides were prepared by co-precipitation method according to two different routes: (i) aqueous solution containing Zr^{4+} and Ce^{4+} from the dissolution of $ZrO(NO_3)_2$ and $Ce(NH_4)_2(NO_3)_6$ precursor salts was added dropwise under vigorous stirring in a buffer solution containing an equi-molar ratio of ammonia and ammonium nitrate solutions (5 mol L^{-1}) (protocol A), or (ii) by continuous addition of droplets of ammonia solution (13 M) into Zr^{4+} and Ce^{4+} solution until complete precipitation (protocol B). The solid thus obtained were dried overnight at 100 °C and then calcined in air at 900 °C for 8 h. The thermal decomposition of the precursor was investigated by calorimetric measurements performed in a TA Instrument DSC-TGA SDT 2960 thermal analyser. X-ray diffraction (XRD) measurements were performed on a Siemens D5000 diffractometer fitted with an anti-cathode CuKα (λ_{Cu} = 1.5406 Å). Raman spectroscopic data were obtained on a Labram Infinity Dilor spectrometer equipped with a frequency-doubled Nd:YAG laser corresponding to an excitation radiation of 532 nm. The silicon line at 521 cm^{-1} was used for calibration before measurements. X-ray photoelectron spectroscopic (XPS) measurements were performed with a Leybold Heraeus spectrometer. Binding energy (B.E.) values were referenced relative to the Zr $3d_{5/2}$ core level at 182 eV. Specific surface area and pore volume measurements were determined from nitrogen physisorption performed at −196 °C on a Micromeritics ASAP 2000 apparatus. Prior to adsorption, all samples were systematically degassed at 300 °C under vacuum.

Temperature-programmed experiments were performed in a fixed bed flow reactor using 1.2 g with a total flow rate of 20 L h^{-1} corresponding to a space velocity of 36,000 h^{-1}. The reactant mixture was typically composed of 2000 ppm N_2O, 1.4 vol.% NO, 1 vol.% O_2 and 15 vol.% H_2O. The outlet gas mixture was analysed with a Shimadzu GC 14A chromatograph fitted with a thermal conductivity detector. Prior to quantification, reactants and products were separated on a CTR1 column supplied by Alltech.

3. Results and discussion

3.1. Bulk and surface properties of freshly prepared $Ce_xZr_{1-x}O_2$ mixed oxides

3.1.1. Bulk characterisation

Particular attention was paid to the influence of experimental route during the precipitation of ceria–zirconia oxy-hydroxides precursors. Fig. 1 reports heat flow profiles recorded during thermal analysis in flowing air from room temperature to 1000 °C on cerium and zirconium hydroxides and oxy-hydroxides precursors obtained from the protocol B. Apparent minima in Fig. 1(a) at 77 and 160 °C, have been assigned to successive endothermic transformations of $Zr(OH)_4$ into amorphous ZrO_2 [26]. The predominant exothermic process at 444 °C is related to the crystallisation of the amorphous ZrO_2 phase into a metastable tetragonal structure [18]. Strong attenuation of the exothermic process at 444 °C related to the crystallisation of tetragonal ZrO_2 and its disappearance is observed with an increase in Ce content. XRD patterns recorded on calcined $Ce_xZr_{1-x}O_2$ samples in air at 900 °C provide further explanations (see Fig. 2). As observed, the most intense X-ray lines at 2θ = 28.2 and 31.5 on ZrO_2 (x = 0) characterise the

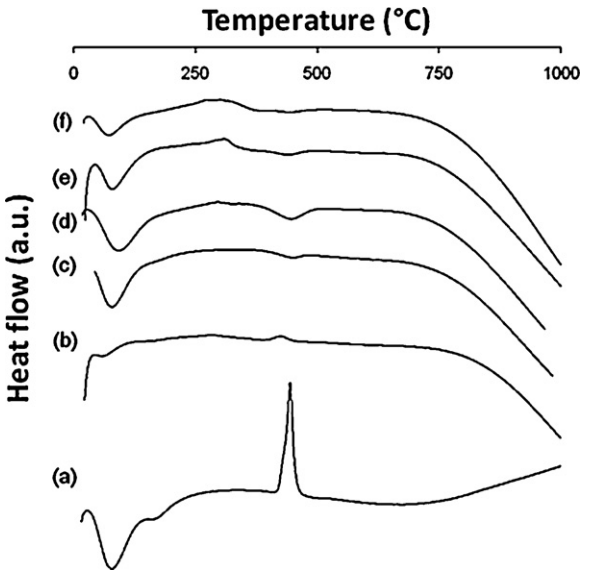

Fig. 1. Heat profiles recorded on $Ce_xZr_{1-x}O_2$ (protocol B) exposed to flowing air from 25 to 1000 °C during thermal analysis (heating rate = 20 °C min^{-1}; mass = 25 mg; total flow rate = 6 L h^{-1}): x = 0 (a); x = 0.15 (b); x = 0.32 (c); x = 0.52 (d); x = 0.75 (e); x = 1 (f).

usual monoclinic structure. Weak signal at 2θ = 30° corresponds to bulk detectable tetragonal zirconia phase in significant lower extent. This XRD line intensifies after ceria incorporation and progressively shifts to lower 2θ values. As seen, a linear relationship can be derived from the plot 2θ vs. atomic Ce composition (x) which emphasizes the fact that possible formation of solid solutions occurs. Cubic CeO_2 with fluorite structure is characterised for x = 1 [22]. Segregation of CeO_2 especially for highly Ce enriched mixed oxides cannot be completely ruled out. Indeed, complex phase diagrams of the CeO_2–ZrO_2 system are usually reported with the occurrence of metastable phases still as a matter of debate [24,25]. Typically, monoclinic symmetry (m) is currently observed for x < 0.1 whereas the stabilisation of the cubic structure (c) usually takes place for x > 0.8. For intermediate compositions the phase diagram of $Ce_xZr_{1-x}O_2$ is unclear with the existence of one stable (t) and two metastable tetragonal phases (t' and t''). The form t'' is recognised as an intermediate between t' and c. The phase boundaries are often approximate because the stabilisation of metastable tetragonal phases strongly depends on the particle size. Crystallite size values calculated for each sample using the Scherrer equation reveal the formation of smaller crystallites for compositions $0.15 \leq x \leq 0.75$ (see Table 1) which emphasize the fact that the sta-

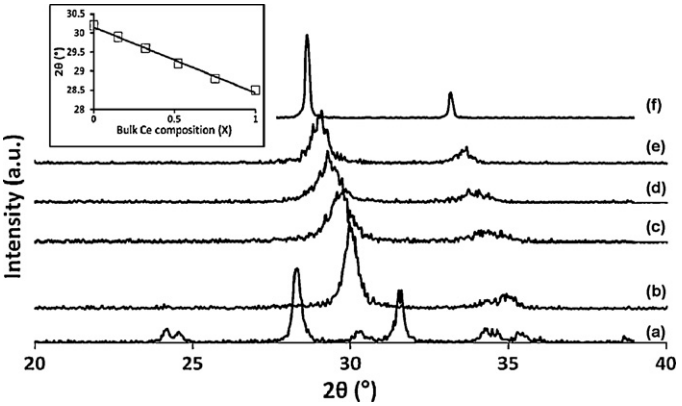

Fig. 2. XRD analysis on $Ce_xZr_{1-x}O_2$ (protocol B) calcined in air at 900 °C: x = 0 (a); x = 0.15 (b); x = 0.32 (c); x = 0.52 (d); x = 0.75 (e); x = 1 (f).

Table 1
Structural properties of ceria, zirconia and ceria–zirconia ($Ce_xZr_{1-x}O_2$) mixed oxides.

Bulk Ce composition	pH	Reference JCPDS data	Structure[a]	Cristallite size (nm)
$x = 1$	A	78-0694	Cubic	83
	B		Cubic	76.4
$x = 0.75$	A	28-0271	Cubic	19.2
	B		Cubic	15.9
$x = 0.52$	A	38-1439	cubic + tetragonal	11.5
	B		cubic + tetragonal	11.2
$x = 0.32$	A	26-0359	Tetragonal	12.5
	B		Tetragonal	11.7
$x = 0.15$	A	80-0785	Tetragonal	18
	B		Tetragonal	19.8
$x = 0$	A	37-1484	Monoclinic + tetragonal	17
	B			24

A: coprecipitation in a buffer solution at constant pH and B: coprecipitation with a gradual increase of pH.
[a] From XRD and Raman observations according to Refs. [31,32].

bilisation of the tetragonal form for $Ce_xZr_{1-x}O_2$ is favoured below a critical particle size [27]. Raman spectroscopy provides complementary information. Spectrum in Fig. 3(a) characterises the typical monoclinic structure of ZrO_2 which should lead to 18 Raman active modes (9Ag + 9Bg) corresponding to the $P21/c$ space group, whereas only 6 Raman active modes (A1g + 2B1g + 3E2g) are expected for a tetragonal structure according to a $P42/nmc$ space group [28]. Finally, only one Raman active mode (F2g) characterises the cubic structure of CeO_2 at 465 cm^{-1} [29,30]. Raman spectra recorded on ceria–zirconia mixed oxides agree with the stabilisation of a tetragonal structure for atomic Ce composition lower than 0.5. On the other hand, the cubic structure coexists for $x \geq 0.52$ as reported elsewhere [31,32] and becomes predominant for atomic Ce composition higher than 0.75. According to earlier explanations [33], the attenuation in intensity of Raman spectra recorded on $Ce_xZr_{1-x}O_2$ could be caused by the presence of oxygen vacancies in higher concentration due to strong interactions between cerium and zirconium oxide species taking place at high calcination temperature. It is also noticeable that Raman lines for $x = 0.32$ (spectrum (c)) shifting to lower wavenumbers could reflect an increase of defect sites as earlier explained [34]. Similar experiments repeated on mixed oxides prepared according to the protocol (A) led to similar observations.

3.1.2. Surface characterisation

Previous convergence on bulk properties has not been observed by examining the surface properties by XPS and N_2 physisorption measurements at −196 °C. As exemplified in Table 2, it is obvious that higher specific surface areas have been usually obtained for mixed oxides in comparison with those measured on single oxides, but this trend seems to be more accentuated by using the protocol (B). Changes in the relative surface Ce composition and in the oxidation state of Zr and Ce were examined by XPS. It was found that the B.E. values of Zr $3d_{5/2}$ core level remained unchanged at 182 eV corresponding to Zr^{4+} species and then was used as internal reference. Ce 3d photopeaks recorded on mixed $Ce_xZr_{1-x}O_2$ usually revealed complex spectral features with the existence of different satellites on the Ce $3d_{5/2}$ and Ce $3d_{3/2}$ core levels. However, no significant change occurs according to the experimental protocols A and B. XPS spectra recorded on the series prepared via the protocol (B) are listed in Fig. 4. Further decomposition leads to the identification of different contributions with the predominance of $u_1(v_1)$, $u_3(v_3)$ and $u_4(v_4)$ which essentially characterises the stabilisation of Ce^{4+}. Nev-

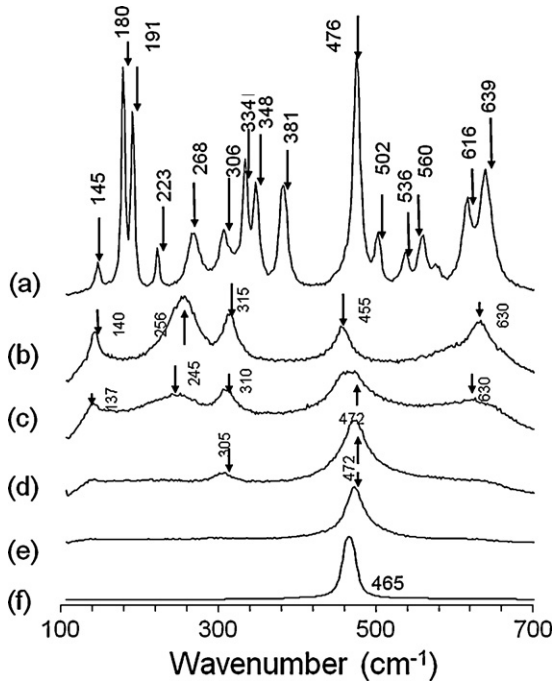

Fig. 3. Raman spectroscopic measurements on $Ce_xZr_{1-x}O_2$ (protocol B) calcined in air at 900 °C: $x = 0$ (a); $x = 0.15$ (b); $x = 0.32$ (c); $x = 0.52$ (d); $x = 0.75$ (e); $x = 1$ (f).

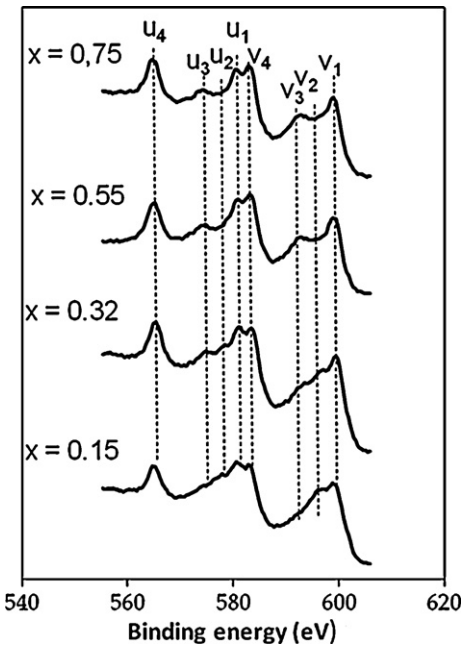

Fig. 4. Ce 3d photopeak from XPS analysis on $Ce_xZr_{1-x}O_2$ (protocol B) calcined in air at 900 °C.

Table 2
Influence of the coprecipitation conditions on the surface properties of calcined $Ce_xZr_{1-x}O_2$ mixed oxides in air at 900 °C: consequences on the catalytic performances in N_2O decomposition.

Bulk Ce composition	pH	SSA ($m^2\,g^{-1}$)	Pore volume (cm^3/g)	XPS analysis		Catalytic performances	
				B.E. Ce $3d_{5/2}$	Surf. Ce conc. (%)	T_{50} (°C)	Specific rate[a]
$x=1$	A	<1	–	–	–	880	~0
	B	<1	–	–	–	880	~0
$x=0.75$	A	1.5	0.007	882.7	0.82	793	4.3×10^{-5}
	B	17.4	0.067	882.3	0.78	670	10.8×10^{-5}
$x=0.52$	A	11	0.038	882.6	0.58	705	3.8×10^{-5}
	B	21.5	0.095	882.2	0.59	660	6.0×10^{-5}
$x=0.32$	A	16.3	0.054	882.5	0.42	710	3.9×10^{-5}
	B	26	0.113	882.8	0.40	670	6.9×10^{-5}
$x=0.15$	A	14.7	0.047	882.6	0.21	730	2.7×10^{-5}
	B	20.7	0.082	882.7	0.22	705	3.4×10^{-5}
$x=0$	A	13	–	–	–	777	1.3×10^{-5}
	B	11	–	–	–	806	1.0×10^{-5}

A: coprecipitation in a buffer solution at constant pH and B: coprecipitation with a gradual increase of pH.
[a] $mol\,h^{-1}\,g^{-1}$ estimated from TPR conversion at 650 °C.

ertheless, one can notice a relative increase in the $u_2(v_2)$ parallel to a decrease in the relative Ce concentration. Such an observation suggests the stabilisation of non-stoichiometric solid solutions for $x \leq 0.5$ due to high calcination temperature but also possibly due to *in situ* photo-reduction of Ce^{4+} to Ce^{3+} currently observed during X-ray irradiation under ultra-high-vacuum. Earlier findings demonstrated that this process is favoured when ceria strongly interacts with a transition metal [35]. Such a photo-reduction is accompanied with a slight shift on the B.E. value of the Ce $3d_{5/2}$ core level towards lower values of approximately 882.3 eV vs. 882.9 eV for bulk CeO_2 [36]. On the other hand, this deviation attenuates for highly Ce loaded samples probably due to more extensive segregation of CeO_2 at the surface. Such an assumption is supported by XPS data reported in Table 2 emphasizing that the relative deviation between bulk and surface Ce composition accentuates with increasing bulk Ce composition.

3.2. Catalytic performances of $Ce_xZr_{1-x}O_2$ in the decomposition of N_2O

The catalytic performances for N_2O decomposition were evaluated from temperature-programmed reaction. The activity of two series of $Ce_xZr_{1-x}O_2$ samples previously prepared according to the protocols A and B was investigated in the presence of 2000 ppm N_2O, 1.4 vol.% NO, 1 vol.% O_2 and 15 vol.% H_2O. NO conversion to NO_2 was only detected in the temperature range 150–400 °C. Above 500 °C, NO oxidation to NO_2 is thermodynamically unfavoured. TPR curves of N_2O conversion to nitrogen are respectively reported in Figs. 5 and 6. In both series a strong synergy effect on the activity is observed due to Ce incorporation to ZrO_2 with a significant shift of the light-off temperature (T_{50}) to lower values irrespective of the nature of the protocol. The following activity sequences can further be established from the T_{50} values (temperature corresponding to 50% N_2O conversion):

- A: $CeO_2 < Ce_{0.75}Zr_{0.25}O_2 < ZrO_2 < Ce_{0.15}Zr_{0.85}O_2 < Ce_{0.32}Zr_{0.68}O_2 < Ce_{0.52}Zr_{0.48}O_2$
- B: $CeO_2 < ZrO_2 < Ce_{0.15}Zr_{0.85}O_2 < Ce_{0.75}Zr_{0.25}O_2 \cong Ce_{0.32}Zr_{0.68}O_2 < Ce_{0.52}Zr_{0.48}O_2$

Different comments arise from those comparisons showing that the protocol B leads to more active catalysts related to higher specific surface areas and to an increase in surface Ce composition. Strictly speaking, no linear relationship between activity and Ce composition can be established for both series and particularly according to the protocol B. In this latter case cerium-doped zirconia catalysts exhibit optimal surface properties for intermediate Ce

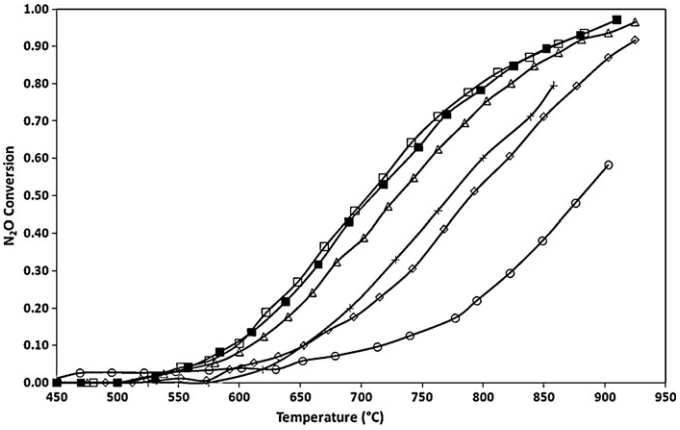

Fig. 5. Temperature-programmed conversion curves during the catalytic decomposition of N_2O on $Ce_xZr_{1-x}O_2$ calcined in air at 900 °C (protocol A): $x=0$ (+); $x=0.15$ (△); $x=0.32$ (■); $x=0.52$ (□); $x=0.75$ (◊); $x=1$ (○).

compositions in the range $x=0.32$–0.52 competing with commercial CeO_2–ZrO_2 mixed oxides in terms of activity (see Fig. 6). A rough estimation of the specific rate at 650 °C also confirms that further increase in Ce composition above 0.52 using the protocol A does not induce subsequent gain in activity but mainly a sharp loss of specific surface area. As a matter of fact, the creation of anionic vacancies in connection with structural properties and surface Ce concentration

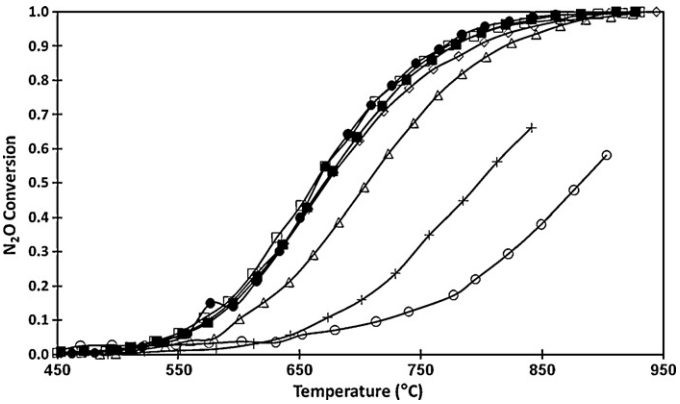

Fig. 6. Temperature-programmed conversion curves during the catalytic decomposition of N_2O on $Ce_xZr_{1-x}O_2$ calcined in air at 900 °C (protocol B): $x=0$ (+); $x=0.15$ (△); $x=0.32$ (■); $x=0.52$ (□); $x=0.75$ (◊); $x=1$ (○); commercial $Ce_xZr_{1-x}O_2$ supplied by Mel Chemical containing 17.5% CeO_2 (●).

probably governs the extent of activity. As indicated, XPS characterised the presence of Ce^{3+} after Ce incorporation. The replacement of Zr^{4+} by Ce^{3+} cations yields solid solutions with higher ionic conduction and oxygen diffusion related to the formation of anionic vacancies which act as charge compensating defect. Previous investigations shown that the distortion of O^{2-} sub-lattices originates a higher oxygen mobility which is not restricted to the surface but also involved bulk oxygen species for $Ce_xZr_{1-x}O_2$ preserving a high residual activity even for highly loaded samples in spite of a quasi-complete loss of specific surface area according to the protocol A [37]. Similar observations have been earlier observed on yttria-modified zirconia with an optimum in the ionic conductivity reaching a maximum in the range 1–10 mol% Y_2O_3 in ZrO_2 [36]. Loss of ionic conductivity for highly loaded samples has been related to various phenomena involving defect interactions, clustering effects and/or local disorder/order transitions which may be restricted to the near-surface region. When the amount of those defects exceeds a critical value then structural reconstructions may occur yielding more ordered structures less active towards the decomposition of N_2O. Returning to highly Ce loaded, XPS observations show greater extent of surface Ce enrichment which can be in connection with a partial segregation of CeO_2. The higher sensitivity of CeO_2 to thermal sintering might explain the loss of specific surface area for $x > 0.52$. A volcano-type influence in the decomposition of N_2O with a maximum corresponding to atomic Ce/Zr ratio was earlier observed by Centi et al. [38]. These authors also suggested that anionic vacancies are involved in the mechanism of the conduction and may also act in the catalytic process. According to Centi et al. [38], an extensive formation of defects or anionic vacancies in $Ce_xZr_{1-x}O_2$ with high Ce loading probably induces structure reconstructions into more ordered defects. Subsequent segregation of CeO_2 at the surface would partly inhibit the catalytic decomposition of N_2O due to extensive thermal sintering further lowering the bulk diffusion of lattice oxygen.

4. Conclusion

The catalytic performances of cerium-doped zirconia catalysts prepared by coprecipitation have been investigated in the decomposition of N_2O at high temperature. A promotional effect on the catalytic activity is observed on $Ce_xZr_{1-x}O_2$ compared with the corresponding Ce and Zr monometallic oxides mainly ascribed to an increase in the specific surface area. An optimal Ce composition also appears for $x = 0.32–0.52$. Ce-enriched mixed oxides exhibit lower activity in N_2O decomposition ascribed to the segregation of CeO_2 more sensitive to thermal sintering. Hence, surface reconstructions occurring on Ce-enriched mixed oxides could lead to more ordered defects above a critical Ce composition in connection with a loss of activity. Such a tendency seems to be closely related to the synthesis route, the protocol B minimising the loss of interaction between Ce and Zr at high Ce content.

References

[1] F. Kapteijn, J. Rodriguez-Mirasol, J.A. Moulijn, Appl. Catal. B 9 (1996) 25.
[2] J. Pérez-Ramirez, F. Kapteijn, K. Schöffel, J.A. Moulijn, Appl. Catal. B 44 (2003) 117.
[3] J. Pérez-Ramirez, F. Kapteijn, G. Mul, X. Xu, J.A. Moulijn, Catal. Today 76 (2002) 325.
[4] S. Alini, F. Basile, S. Blasioli, C. Rinaldi, A. Vaccari, Appl. Catal. B 70 (2007) 323.
[5] M. Santiago, J. Pérez-Ramirez, Environ. Sci. Technol. 41 (2007) 1704.
[6] J. Pérez-Ramirez, M. Santiago, Chem. Commun. (2007) 619.
[7] B. Coq, M. Mauvezin, G. Delahay, J.-B. Butet, S. Kieger, Appl. Catal. B 27 (2000) 193.
[8] A. Guzman-Vargas, G. Delahay, B. Coq, Appl. Catal. B 42 (2003) 369.
[9] J.P. Dacquin, M. Cabié, C.R. Henry, C. Lancelot, C. Dujardin, S.R. Raouf, P. Granger, J. Catal. 270 (2010) 299.
[10] G. Centi, G. Cerrato, S. D'Angelo, U. Finardi, E. Giamello, C. Morterra, S. Perathoner, Catal. Today 27 (1996) 265.
[11] C. Monterra, E. Gianello, G. Cerrato, G. Centi, S. Perathoner, J. Catal. 179 (1998) 111.
[12] J.P. Dacquin, C. Dujardin, P. Granger, Catal. Today 137 (2008) 390.
[13] P. Stelmachowski, F. Zasada, G. Maniak, P. Granger, M. Inger, M. Wilk, A. Kotarba, Z. Sojka, Catal. Lett. 130 (2009) 637.
[14] J.P. Dacquin, C. Dujardin, P. Granger, J. Catal. 253 (2008) 37.
[15] Ø. Nirisen, K. Schöffel, D. Waller, D. Øvrebø, World Patent 0202230 A1 (2002).
[16] B. Neveu, C. Hamon, World Patent 9964139 (1999).
[17] F. Van Deyck, F.J. Weiss, R. Verbeck, E. Thomas, B. Monghelshots, P. Pijl, US Patent 4,507,271 (1985).
[18] P. Granger, P. Esteves, S. Kieger, L. Navascues, G. Leclercq, Appl. Catal. B 62 (2005) 236.
[19] M. Ruzak, M. Inger, S. Witkowski, M. Wilk, A. Kotarba, Z. Sojka, Catal. Lett. 126 (2008) 72.
[20] G. Giecko, T. Borowiecki, W. Gac, J. Kruk, Catal. Today 137 (2008) 403.
[21] W.J. Stark, M. Maciejewski, L. Mädler, S.E. Pratsinis, A. Baiker, J. Catal. 220 (2003) 35.
[22] S. Damyanova, C.A. Perez, M. Schmal, J.M.C. Bueno, Appl. Catal. A 57 (1990) 127.
[23] S. Rossignol, Y. Madier, D. Duprez, Catal. Today 50 (1999) 261.
[24] J. Kašpar, P. Fornasiero, M. Graziani, Catal. Today 50 (1999) 285.
[25] T. Montini, A. Speghini, L. De Rogatis, B. Lorenzut, M. Bettinelli, M. Graziani, P. Fornasiero, J. Am. Chem. Soc. 131 (2009) 13155.
[26] C. Bozo, N. Guilhaume, E. Garbowski, M. Primet, Catal. Today 59 (2000) 33.
[27] R.C. Garvie, J. Phys. Chem. 82 (1978) 219.
[28] M. Yashima, K.H. Arashi, M. Kakihana, M. Yoshimura, J. Am. Ceram. Soc. 77 (1994) 1067.
[29] M. Yashima, K. Morimoto, N. Ishizawa, M. Yoshimura, J. Am. Ceram. Soc. 76 (1993) 2865.
[30] V.G. Keramidis, W.B. White, J. Am. Ceram. Soc. 57 (1974) 22.
[31] G. Colon, M. Pijolat, F. Valdivieso, H. Vidal, J.K. Kašpar, M. Daturi, C. Binet, J.C. Lavalley, R.T. Blake, S. Bernal, J. Chem. Soc. Faraday Trans. 94 (1998) 3717.
[32] T. Murota, T. Hasagawa, S. Aozasa, H. Matsui, M. Motoyama, J. Alloys Compd. 193 (1993) 298.
[33] P. Fornasiero, G. Balducci, R. Di Monte, J. Kaspar, V. Sergo, G. Gubitosa, A. Ferrero, M. Graziani, J. Catal. 164 (1996) 173.
[34] D. Kim, H. Jung, I. Yang, J. Am. Ceram. Soc. 76 (1993) 2106.
[35] P. Granger, J.F. Lamonier, N. Sergent, A. Aboukais, L. Leclercq, G. Leclercq, Top. Catal. 16/17 (1–4) (2001) 89.
[36] C.E. Guillaume, M. Vermeersh, R. Sporken, J.J. Verbist, S. Mathot, G. Demortier, Surf. Interface Anal. 22 (1994) 186.
[37] S. Lemaux, A. Bensaddik, A.M.J. van der Eerden, D.C. Koningsberger, J. Phys. Chem. B 105 (2001) 4810.
[38] G. Centi, S. Perathoner, Z.S. Rak, Appl. Catal. B 41 (2003) 143.